

Effects of excitation light polarization on fluorescence emission in two-photon light-sheet microscopy

Giuseppe de Vito^{a,b}, Pietro Ricci^b, Lapo Turrini^{b,c}, Natascia Tiso^d, Francesco Vanzi^{b,e}, Ludovico Silvestri^{b,c,f}, Francesco Saverio Pavone^{b,c,f,*}

^aUniversity of Florence, Department of Neuroscience, Psychology, Drug Research and Child Health, Viale Pieraccini 6, Florence, Italy, 50139

^bEuropean Laboratory for Non-Linear Spectroscopy, Via Nello Carrara 1, Sesto Fiorentino, Italy, 50019

^cUniversity of Florence, Department of Physics and Astronomy, Via Sansone 1, Sesto Fiorentino, Italy, 50019

^dUniversity of Padova, Department of Biology, Via Ugo Bassi 58/B, Padua, Italy, 35131

^eUniversity of Florence, Department of Biology, Via Madonna del Piano 6, Sesto Fiorentino, Italy, 50019

^fNational Institute of Optics, National Research Council, Via Nello Carrara 1, Sesto Fiorentino, Italy, 50019

Abstract

Significance

Light-sheet microscopy (LSM) is a powerful imaging technique that uses a planar illumination oriented orthogonally to the detection axis. Two-photon (2P) LSM is a variant of LSM that exploits the 2P absorption effect for sample excitation. The light polarization state plays a significant, and often overlooked, role in 2P absorption processes.

Aim

The scope of this work is to test whether using different polarization states for excitation light can affect the detected signal levels in 2P LSM imaging of biological samples with a spatially unordered dye population.

Approach

We compared the fluorescence signals obtained using different polarization states with various fluorophores (fluorescein, EGFP and GCaMP6s) and different samples (liquid solution and fixed or living zebrafish larvae).

Results

In all conditions, linear polarization oriented parallel to the detection plane provided the largest signal levels, while perpendicularly-oriented polarization gave low fluorescence signal with the biological samples, but a large signal for the fluorescein solution. Finally, circular polarization generally provided lower signal levels.

Conclusions

These results highlight the importance of controlling the light polarization state in 2P LSM of biological samples. Furthermore, this characterization represents a useful guide to choose the best light polarization state when maximization of signal levels is needed, e.g. in high-speed 2P LSM.

Keywords: light-sheet microscopy; two-photon microscopy; zebrafish imaging; light polarization.

*Francesco Saverio Pavone, E-mail: francesco.pavone@unifi.it

1 Introduction

Light-sheet (LS) fluorescence microscopy is a powerful optical imaging technique¹ based on the principle of a planar illumination oriented orthogonally with respect to the detection axis². It employs wide-field detectors that allow to parallelize the photon collection, thus offering a large increment in the acquisition speed. Moreover, it offers also a good optical section capability and reduced sample photodamage and photobleaching, compared to other optical imaging techniques³.

Two-photon (2P) LS microscopy⁴⁻⁸ is a technique developed from traditional 1-photon (1P) LS microscopy that exploits the 2P absorption effect for sample excitation⁹. The excitation wavelengths used in 2P absorption are usually in the infra-red region: a frequency range

characterized by reduced scattering inside biological tissues compared to visible light¹⁰. This effect, combined with the quadratic dependence of the absorption rate on the excitation light intensity, offers several additional advantages: a larger penetration depth in the sample, a reduction of the sample-induced aberrations, a better uniformity of the illumination distribution and an improved image contrast¹¹.

The polarization state of the excitation light plays a significant, and often overlooked, role both in 1P and 2P absorption processes exploited in microscopy, operating differently in the two cases¹². In particular, in the 2P absorption process, the sum of angular momenta of the absorbed photons is required to be zero, since the total angular momentum change related to the electronic state transition in most fluorophores is null^{13,14}. This is the reason why linearly-polarized light is associated with a higher 2P absorption with respect to circularly-polarized light, since in the former configuration there is a 50% probability for the fluorophore to interact with photons with opposite handedness that can reciprocally compensate their own angular momenta. On the other hand, the use of circularly-polarized light will lead to a spatially more homogeneous fluorophore excitation, whereas in case of linearly-polarized light the excitation probability depends on $\cos^2(\theta)$, for 1P excitation, or $\cos^4(\theta)$, for 2P excitation; where θ is the angle between the polarization axis of the exciting electric field and the dipole moment orientation of the dye molecule¹⁵. This means that when linearly-polarized excitation light is used, a photoselection of the dyes is performed based on their spatial orientation and this effect is much more pronounced with 2P excitation. We illustrated this situation in Fig. 1 that shows a dye emitting fluorescence only when excited with a linearly-polarized light with $\theta \approx 0$.

It should be noted that this situation is different from the case in which the spatial anisotropy is present in the general dye population regardless of the excitation, i.e. when the dye population is spatially ordered due to the inherent biological properties of the sample. In the latter case polarization-resolved 1P or 2P fluorescence microscopy can be used to extract important information about the sample micro-architecture^{16–19}; however, in the present work we will focus on the more general case in which the native population of fluorophores is supposed to be randomly oriented.

The fact that, when using linearly-polarized excitation light, the population of excited dyes is spatially anisotropic induces a spatial anisotropy also in fluorescence emission. This is because the fluorescence emission happens preferentially on an axis perpendicular with respect to the emission transition moment¹⁵ (the latter can be grossly approximated as parallel with the absorption transition moment for many dyes). The effects of this spatial anisotropy, as well as of the ellipticity of the excitation light, on biological imaging of randomly-oriented dyes were already experimentally characterized for 1P confocal microscopy and 2P microscopy¹³. Nevertheless, their characterization is still lacking for LS microscopy, where the different geometry of the excitation and detection optical axes makes the presence of this anisotropy even more significant. We illustrated this situation in Fig. 1. As it is shown, the different orientationally-defined dye populations photoselected by the polarization directions of the excitation light preferentially emit light toward different directions. This means that the polarization orientation of the excitation light could in principle be experimentally orientated as to maximize the light emitted toward the direction of the detection objective in a LS microscope.

The described situation assumes the time-scale of the dye rotational movement being much slower than the fluorescence life-time, meaning that the orientation population of the excited

dyes could not randomize before the photon emission. This does not represent the general case, since in liquid solution the majority of fluorophores can rotate in a time-scale of $50 \div 100$ ps, while the fluorescence life-time is usually in the time scales of $1 \div 10$ ns¹⁵. On the other hand, rotational diffusion is limited in viscous media, such as biological tissues. In addition to medium viscosity, the rotational diffusion can be mitigated also by bonded molecules which damp the free rotational movement of the fluorophore. This can be relevant when the fluorophore is actually an internal moiety of a large bio-macromolecule, such as the Green Fluorescent Protein (GFP), or when it non-covalently interacts with larger biological molecules.

In general, there are several environment factors relevant in a biological sample context that can bring the rotational time-scale to be comparable to typical fluorescence life-times, thus affecting the anisotropy of the excited dye population and therefore of the spatial fluorescence emission.

Therefore, the scope of this work is to test whether the use of different polarization states for the excitation light (circular polarization or linear polarization, with two orthogonal polarization orientations) can affect the detected signal levels when performing 2P LSM of biological samples in which the dyes are randomly oriented.

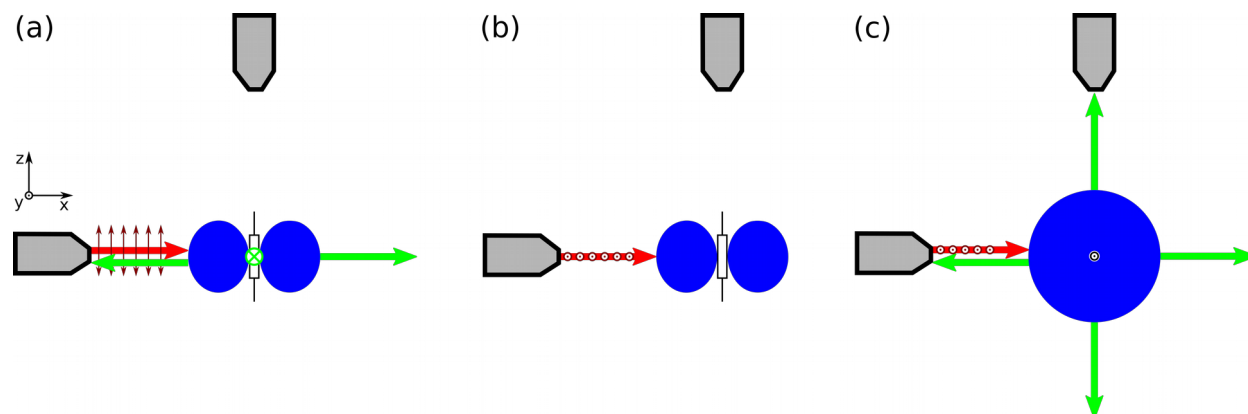


Fig. 1 Schematic of the polarization-dependent effects in 2P LS microscopy neglecting the fluorophores rotational movements. (a) If both the polarization plane (indicated by dark-red arrows) of the linearly-polarized excitation light (red arrow) and the transition dipole of the fluorophore (in blue) are aligned with the z-axis, the fluorophore is excited, but the fluorescence light (green arrows) is emitted predominately on the xy-plane. (b) If the polarization plane of the excitation light is parallel to the y-axis while the transition dipole is perpendicular to it, then no fluorescence light is generated. (c) If both the polarization plane of the excitation light and the transition dipole are aligned with the y-axis, then the fluorescence light is emitted predominately on the xz-plane and therefore it can be collected by the detection objective (on the top).

2 Methods

We used two strains of transgenic zebrafish (*Danio rerio*) larvae: 3 Tg(elavl3:H2B-GCaMP6s) larvae^{20,21} in homozygous *albino* background²² and 6 Tg(actin:EGFP) larvae²³. The former expresses, with nuclear localization, the fluorescent calcium sensor “GCaMP6s” under a pan-neuronal promoter, while the latter expresses enhanced GFP (EGFP) in all tissues owing to a ubiquitous promoter. Zebrafish strains were maintained according to standard procedures²⁴. To avoid skin pigment formation, Tg(actin:EGFP) larvae were raised in 0.003% N-phenylthiourea (P7629, Sigma-Aldrich). All larvae were observed at 4 days post fertilization (dpf). Fish maintenance and handling were carried out in accordance with European and Italian law on

animal experimentation (D.L. 4 March 2014, no. 26), under authorization no. 407/2015-PR from the Italian Ministry of Health.

Five of the larvae were subjected to live imaging. Immediately before the acquisition, each larva was anesthetized with a solution of tricaine (160 mg/L; A5040, Sigma-Aldrich), was included in 1.5% (w/v) low gelling temperature agarose (A9414, Sigma-Aldrich) in fish water (150 mg/L Instant Ocean, 6.9 mg/L NaH_2PO_4 , 12.5 mg/L Na_2HPO_4 , pH 7.2), and mounted on a custom-made glass support immersed in fish water thermostated at 28.5 °C. The other 4 larvae were fixed (2h in 4% paraformaldehyde in PBS at room temperature) before undergoing the same mounting procedure.

The imaging was performed with a custom-made 2P LS microscope. The setup scheme is shown in Fig. 2. Excitation light at 930 nm is generated by a pulsed Ti:Sa laser (Chameleon Ultra II, Coherent) and a pulse compressor is employed to pre-compensate for the group delay dispersion (PreComp, Coherent). The beam is attenuated using a half-wave plate and a Glan-Thompson polarizer and then it passes through an Electro-Optical Modulator used to rotate on command its linear polarization plane by 90°. Moreover, we use a combination of a half-wave plate and a quarter-wave plate to align the light polarization plane with the reference system of the microscope and to pre-compensate for the polarization distortions. The beam is then scanned by a fast resonant galvanometric mirror (CRS-8 kHz, Cambridge Technology), used to generate the digitally-scanned LS along larval rostro-caudal direction, while a closed-loop galvanometric mirror (6215H, Cambridge Technology) is used to scan the LS along larval dorso-ventral direction. The beam is finally relayed to an excitation dry objective (XLFLUOR4X/340/0,28, Olympus), placed at the lateral side of the larva, by a scan-lens (50 mm focal length), a tube-lens (75 mm focal length) and a pair of relay lenses (250 mm and 200 mm focal lengths) that underfill the objective pupil. When needed, we converted the light polarization state from linear to circular by placing a removable quarter-wave plate on the beam-path between the tube lens and the first relay lens.

The emitted green fluorescent light, coming either from GCaMP6s or EGFP, is collected by a water-immersion objective (XLUMPLFLN20XW, Olympus) placed dorsally above the larva. The objective is scanned along the axial dimension by an objective scanner (PIFOC P-725.4CD, Physik Instrumente) synchronously with the closed-loop galvanometric mirror movements. The optical image formed by the detection-objective tube lens (300 mm focal length) is then demagnified by exploiting a second pair of tube lens (200 mm focal length) and objective (UPLFLN10X2, Olympus), bringing the final magnification to 3×. Finally, the green fluorescence is spectrally filtered (FF01-510/84-25 nm BrightLine® single-band bandpass filter, Semrock) and relayed to a sCMOS camera (ORCA-Flash4.0 V3, Hamamatsu).

Imaging was performed with a pixel size of about $2 \times 2 \mu\text{m}^2$, and a field of view of about $1 \times 1 \text{ mm}^2$. The acquisitions in fluorescein solution were performed on a single transversal plane with an exposure time of 100 ms. The larvae instead were imaged with volumetric acquisitions composed by 31 planes spaced by 5 μm and with an exposure time of 26 ms for each plane and a volumetric acquisition frequency of 1 Hz (~200 ms where reserved for objective flyback time). Each acquisition lasted 1 minute and then the 60 acquired volumetric stacks were averaged to obtain one final z-stack.

The laser power used for the acquisitions, measured at the excitation objective pupil, was 100 mW for the Tg(actin:EGFP) larvae both in living and fixed preparations, 200 mW for the live

imaging of Tg(elavl3:H2B-GCaMP6s) larvae, 180 mW for the fixed Tg(elavl3:H2B-GCaMP6s) larvae and 162 mW for the fluorescein solution acquisition. Great care was taken to ensure that the excitation power remained constant when imaging with the three different polarizations. Moreover, we checked that this power range is far from the fluorescence saturation regime by measuring the average fluorescent signal generated by a fixed Tg(actin:EGFP) larva while varying the excitation power from 25 mW to 525 mW. The results, shown in Fig. S1 in the Supplemental Materials, clearly depict a quadratic dependence of the signal from the excitation power (coefficient of determination: 0.999), as expected in 2P microscopy, and therefore we can exclude the presence of a saturation effect.

Before each acquisition session, we monitored the residual polarization distortions by temporarily inserting on the beam-path a half-wave plate followed by a Glan–Thompson polarizer before the excitation objective pupil. We then manually rotated the retarder while measuring the power variation after the polarizer. For circularly polarized light the amplitude of the observed oscillations was less than 4% of the signal.

General linear mixed models were used to analyze the results for the Tg(actin:EGFP) larvae and the fixed Tg(elavl3:H2B-GCaMP6s) larvae. The models were implemented with the library “lmerTest”²⁵ for the R language for statistical computing. We used the fluorescent signal as dependent variable, the polarization state as fixed effect and the fish as random effect. A linear regression model implemented in R language was instead used to analyze the results for the living Tg(elavl3:H2B-GCaMP6s) larva. We used the fluorescent signal as dependent variable and the polarization state and the Region Of Interest (ROI) as independent variables. In both cases we used linear contrasts to compare the polarization groups and we used the Sidak method for the multiplicity correction. Fluorescein solution data were compared by computing 95% Confidence Intervals (C.I.) using the Student's t-distribution. In the following, all the fluorescence signal values are expressed in Arbitrary Units (A.U.).

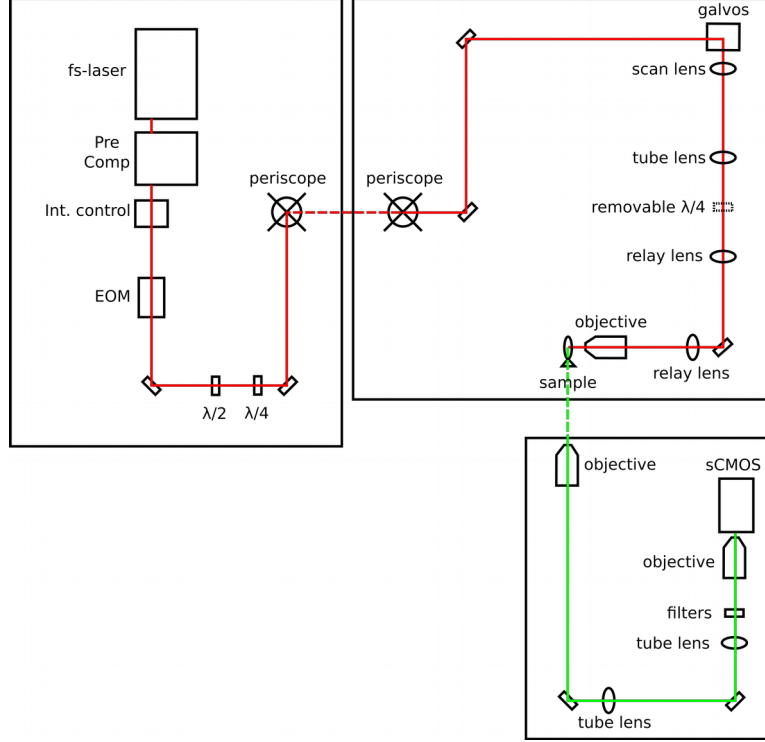


Fig. 2 Schematic of the custom-made 2P LS microscope. Fs-laser: femtosecond laser. Pre Comp: pulse compressor. Int. control: intensity control assembly, composed by a half-wave plate and a Glan–Thompson prism. EOM: Electro-Optical Modulator. $\lambda/2$: half-wave plate. $\lambda/4$: quarter-wave plate. Galvos: galvanometric mirror assembly, composed by a resonant mirror and a closed-loop mirror. Red line: excitation light. Green line: fluorescence light. The dashed lines indicate vertical paths.

3 Results and discussion

In a medium where the fluorophores are able to rotate completely unrestrained, we would expect the fluorescence emission to be isotropic, because in this condition the thermally induced rotation movements happen on time scales much shorter than fluorescence lifetime, as discussed in Sec. 1.

To test this hypothesis, we excited fluorescence in a high-concentrated fluorescein solution employing linearly- and circularly-polarized light, and we show the results in Fig. 3. The polarization plane of the former was aligned either parallel or perpendicular to the plane where the optical axes of the detection and excitation objectives lay; in the following we shall refer to the parallel condition as “vertical polarization” and the perpendicular condition as “horizontal polarization” (corresponding to the z-axis and the y-axis in Fig. 1, respectively).

We indeed observed similar fluorescence levels when employing vertically- or horizontally-polarized light, nevertheless we revealed a small, albeit statistically significant, difference between the two polarization states: the signal in horizontal-polarization condition (544.7 A.U.; 95% C.I.: [539.2, 550.2] A.U.) is ~3% larger with respect to the vertical-polarization condition (529.5 A.U.; 95% C.I.: [527.6, 531.5] A.U.). This observation indicates that even in a medium that favors high-level of molecular mobility, as in solution, the fluorophores can still exhibit a residual degree of spatial anisotropy in their fluorescence emission. A much larger difference was instead observed for circularly-polarized light: for this condition, we observed a ~30% reduction

in the fluorescence signal level (374.4 A.U.; 95% C.I.: [372.0, 376.8] A.U.) with respect to the two linear polarization conditions. This is consistent with the low 2P excitation efficiency that characterizes the circular polarization. Nevertheless, it is not a trivial result, since circular polarization can excite the dyes in a spatially-homogeneous fashion, while the linearly-polarized light can excite only the subset of dyes that are almost parallel to its polarization-plane, as discussed in Sec. 1. This result therefore indicates that the widening of the group of possible target dyes is not sufficient to compensate the decrease in excitation efficiency for the circular polarization with respect to the linear polarization.

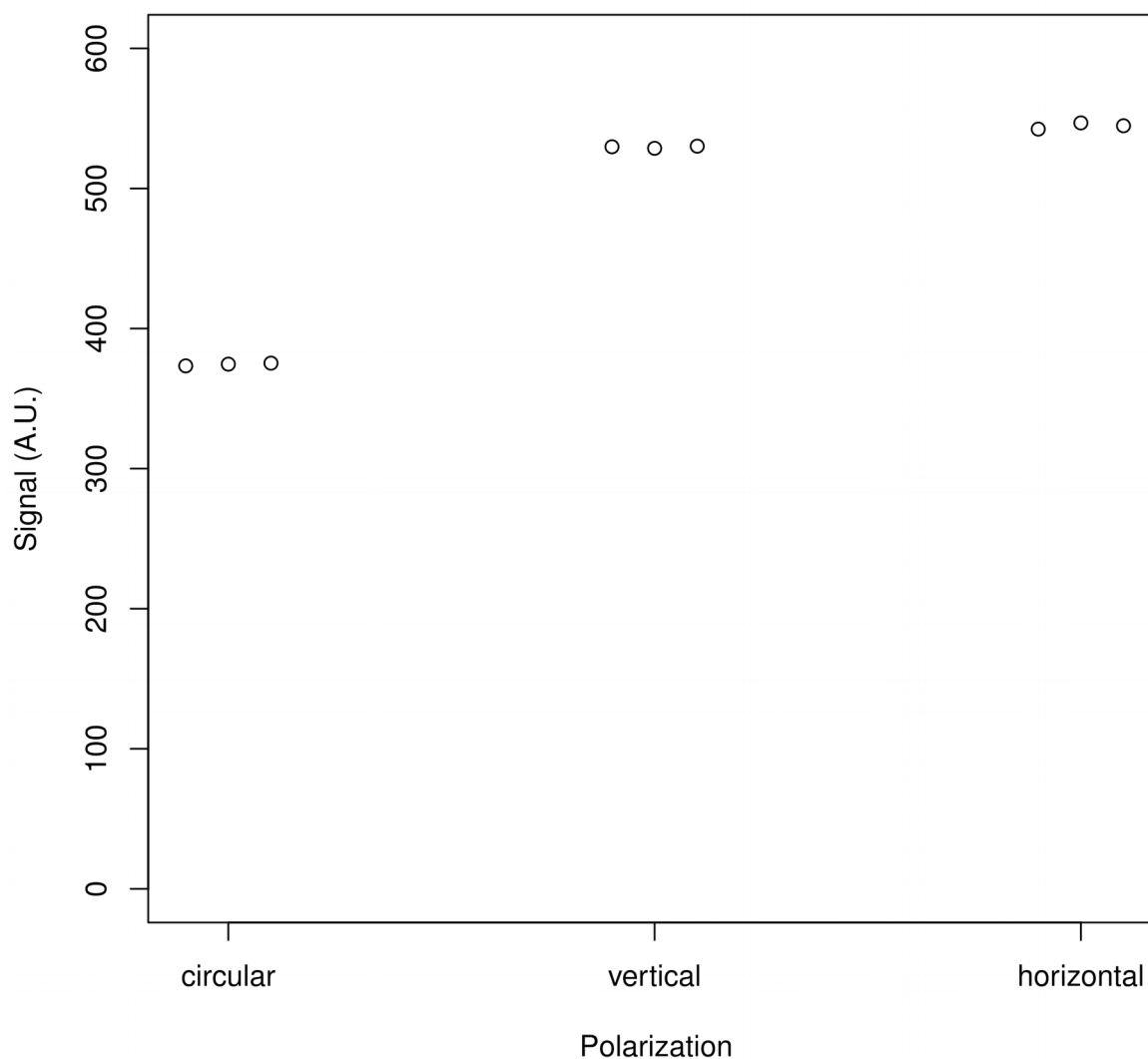


Fig. 3 Scatter plot of the signal generated by a fluorescein solution excited with circularly-, vertically- or horizontally-polarized light. Each condition was tested in triplicate and each point represents a single measure.

We then tested if this polarization-dependent effect is present also in tissue imaging. To do so, we observed zebrafish larvae expressing EGFP, both in fixed and in living conditions, and we show the results in Fig. 4. In this case, we selected an arbitrary ROI for each larva (as depicted in Figs. 4(a) and 4(b)) and we measured its mean fluorescence signal. In this case, we did not observe significant differences between the circular-polarization condition and the vertical-polarization condition in both the fixed (41.6 A.U., standard deviation: 15.3 A.U. and 45.0 A.U., standard deviation: 14.2 A.U., respectively) and the living (53.4 A.U., standard deviation: 18.8 A.U. and 48.9 A.U., standard deviation: 17.5 A.U., respectively) conditions. We observed instead a large and significant (p -value < 0.0001) signal increase in the horizontal-polarization condition with respect to the circular- and the vertical-polarization conditions, both in the fixed-condition ($\sim 67\%$ and $\sim 54\%$, respectively; horizontal-polarization value: 69.3 A.U., standard deviation: 20.4 A.U.) and in the living condition ($\sim 41\%$ and $\sim 54\%$, respectively; horizontal-polarization value: 75.2 A.U., standard deviation: 29.2 A.U.).

It should be noted how in the animal tissue the difference in the signal levels between the horizontal- and the vertical-polarization conditions is much more marked with respect to the fluorescein solution. We hypothesize that this effect could be ascribed to the different molecular rotational mobility in the two environments.

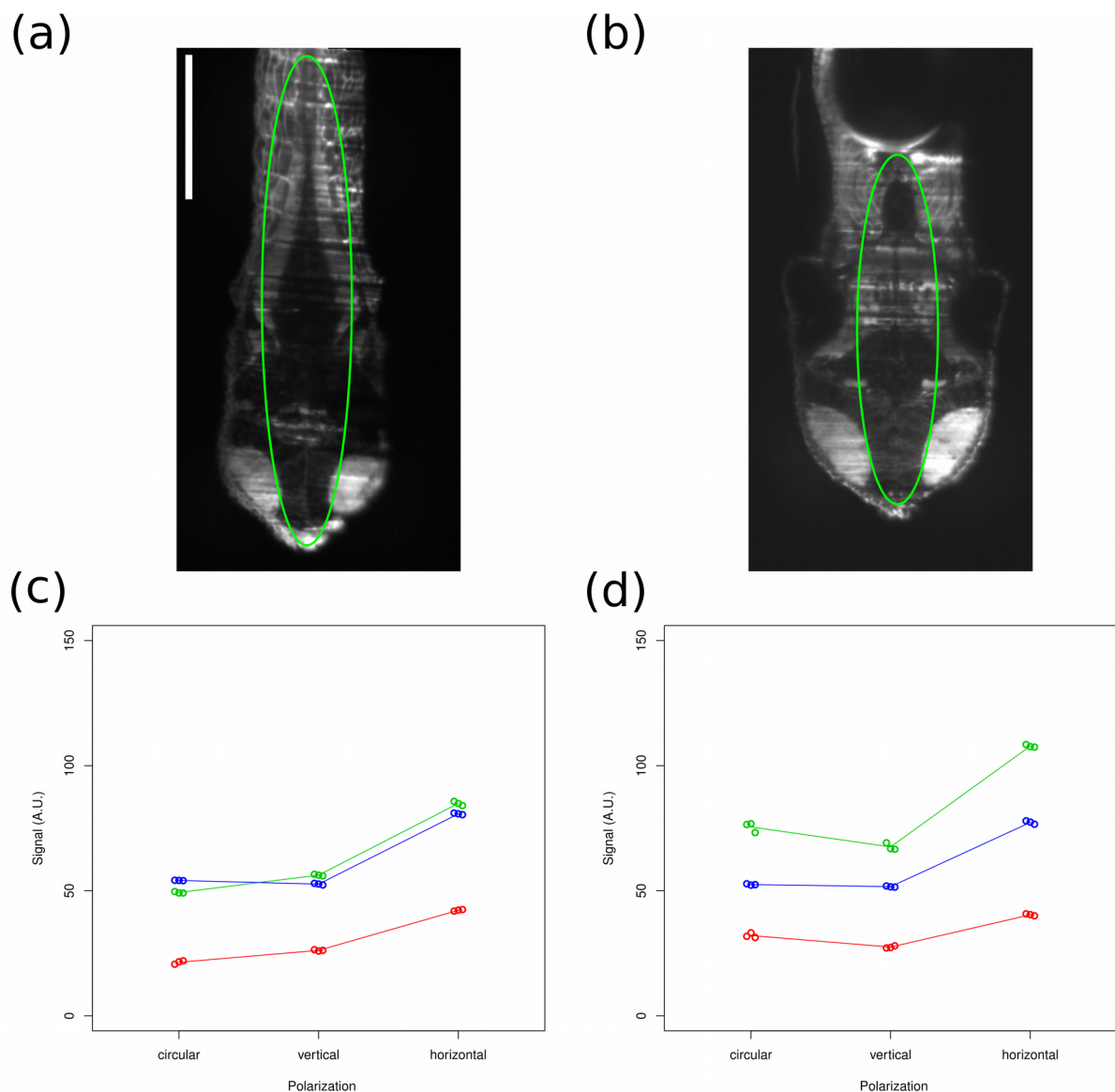


Fig. 4 Imaging of Tg(actin:EGFP) larvae in fixed condition, (a) and (c), and in living condition, (b) and (d). (a) and (b): individual z-slices extracted from the volumetric acquisitions of larvae representative of the respective conditions. The green ovals indicate the ROIs traced on these larvae. Scale bar: 100 μ m. (c) and (d): scatter plots of the average signal measured from the ROIs as a function of the polarization condition. Each point represents an individual acquisition, the points inherent to the same animal are indicated with the same color in the respective graph. The average values for each animal and for each condition are linked with lines of the same color.

Finally, we tested if this polarization-dependent effect can be observed also with a fluorescent calcium indicator, such as GCaMP6s. For the fixed-condition, we measured the average fluorescence signal emitted by arbitrarily selected ROIs, similarly to what we did for the EGFP experiments, and we show the results in Figs. 5(a) and 5(c).

Also in this case, we did not observe a significant difference between the circular-polarization condition (14.5 A.U., standard deviation: 1.1 A.U.) and the vertical-polarization (15.5 A.U., standard deviation: 1.3 A.U.) conditions. However, the measured fluorescence levels

in the horizontal-polarization condition (26.5 A.U., standard deviation: 1.5 A.U.) showed a large and significant (p-value < 0.0001) increase with respect to the circular-polarization condition (~83%) and the vertical-polarization condition (~71%).

We tested if the GCaMP6s polarization-dependent effect can be observed also during live-imaging. These measures are different with respect to the previous ones, since the cellular calcium levels, and therefore the emitted fluorescence, vary during the time, reflecting the time-dependent neuronal activity. In particular, this means that, due to the fluctuations in basal neuronal activity, the fluorescence levels change in the time needed to switch the polarization state. For this reason, we decided to draw ROIs around individual neuronal cells (i.e. the individual sources of the time-dependent signal), and we show the results in Figs. 5(b) and 5(d).

In this case we did not observe a significant difference between the circular-polarization condition (3.6 A.U., standard deviation: 1.9 A.U.) and the vertical- (2.1 A.U., standard deviation: 1.4 A.U.) and the horizontal-polarization (4.8 A.U., standard deviation: 3.5 A.U.) conditions. However, we observed a large (~128.6%) and significant (p-value=0.0016) increase in the fluorescence signal level in the horizontal-polarization condition with respect to the vertical-polarization condition.

The slightly different trends observed for GCaMP6s between the fixed and the living conditions could be ascribed to several factors. The fixation procedure induces cross-linking between molecules that could alter the rotational mobility of the fluorophore. Moreover, the physico-chemical properties of the cytosol change between the living and the fixed states and this medium alteration could affect the motion of the dye. Finally, the fine spatio-temporal biological control of the calcium distribution is completely abolished in the fixed state and therefore also the distribution between the bound and the unbound states of the fluorescent sensor is altered in the two cases, affecting its fluorescence characteristics.

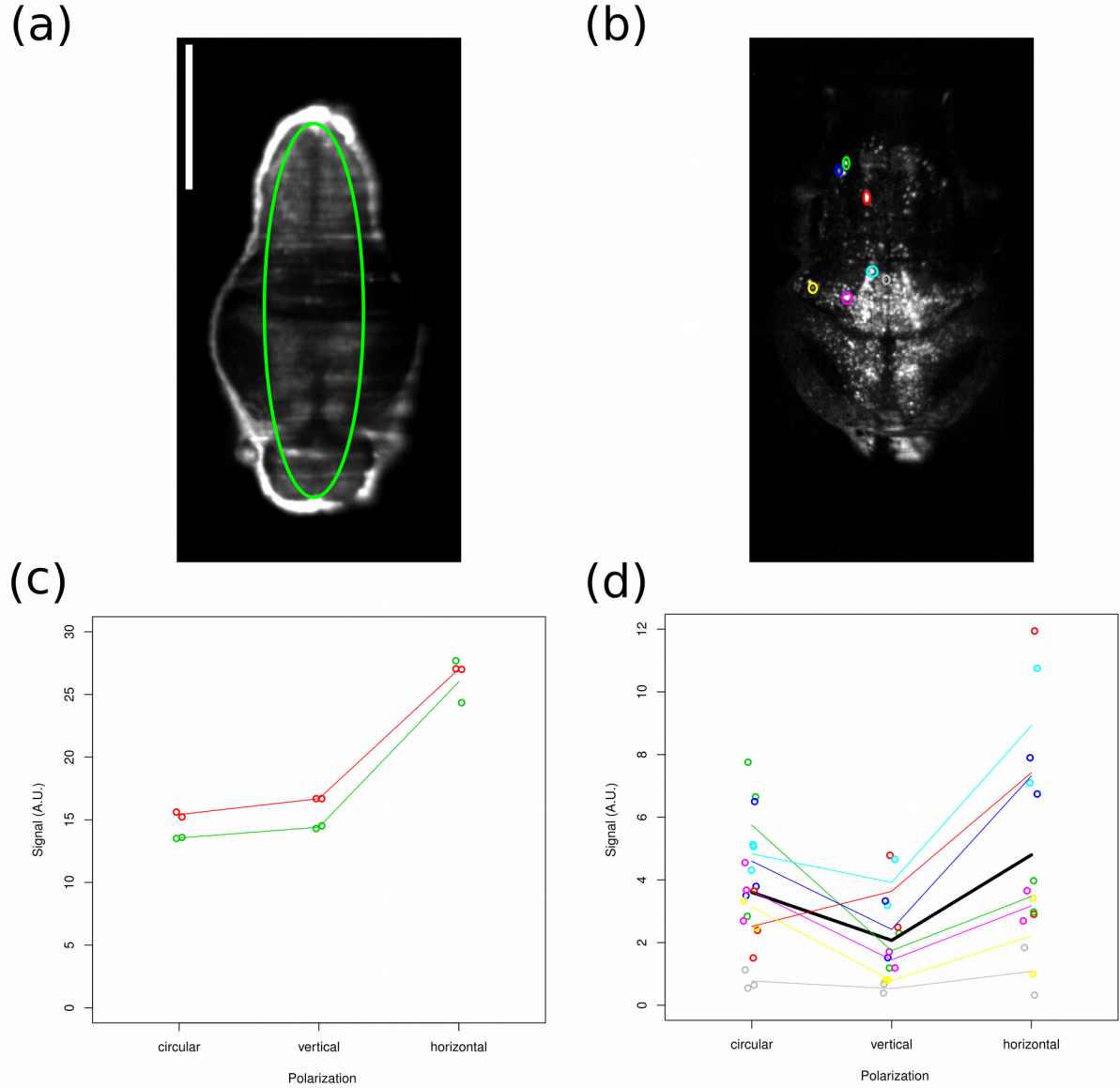


Fig. 5 Imaging of Tg(elavl3:H2B-GCaMP6s) larvae in fixed condition, (a) and (c), and in living condition, (b) and (d). (a): individual z-slice extracted from the volumetric acquisitions of a representative larva. The green oval indicate the ROI measured for this larva. (b): maximum projection of a sub-volume of the volumetric stack (70 μm along the dorso-ventral direction from the original 150 μm) of the larva. The colored ovals indicated the different ROIs. Scale bar: 100 μm . (c) and (d): scatter plots of the average signal measured from the ROIs traced on the larvae as a function of the polarization condition. (c): each point represents an individual acquisition, the points inherent to the same animal are indicated with the same color. The average values for each animal and for each condition are linked with lines of the same color. (d): different colors indicate different ROIs, as shown in (b). For each color, each point represents an individual acquisition. The average values for each ROI and for each condition are linked with lines of the same color. The thick black line indicates the global averages for each condition.

4 Conclusions

In this work we compared the fluorescence signal levels obtained using different excitation light polarization states with various fluorophores and different samples in 2P LSM. In all the different

conditions tested, horizontal polarization proved to provide the largest signal levels, while circular polarization generally provided low signal levels. Moreover, vertical polarization gave low fluorescence signal levels with all the biological samples, albeit it provided a large signal for the fluorescein solution. Taken together, these results highlight the importance of controlling the polarization state of the excitation light in 2P LSM of biological samples.

Furthermore, this characterization represents a useful guide to choose the properly-oriented linearly-polarized light when maximization of signal levels is needed. This is particularly important in high-speed 2P LSM, because in this situation (differently from 1P LSM) the acquisition frequency is usually limited by the signal-to-noise ratio and therefore increasing the signal levels is necessary to achieve a higher temporal resolution.

Disclosures

The authors declare that there are no conflicts of interest related to this paper.

Acknowledgments

This project has received funding from the European Research Council (ERC) under the European Union's Horizon 2020 research and innovation programme (grant agreement No 692943)

References

1. J. Huisken et al., "Optical Sectioning Deep Inside Live Embryos by Selective Plane Illumination Microscopy," *Science* **305**(5686), 1007–1009 (2004) [doi:10.1126/science.1100035].
2. H. Siedentopf and R. Zsigmondy, "Visualisation and determination of size of ultra microscopic particles, with special use of Goldrubin glasses," *Annalen der Physik* **10**(1), 1–39 (1902).
3. P. A. Santi, "Light Sheet Fluorescence Microscopy: A Review," *J Histochem Cytochem.* **59**(2), 129–138 (2011) [doi:10.1369/0022155410394857].
4. T. V. Truong et al., "Deep and fast live imaging with two-photon scanned light-sheet microscopy," *Nat Methods* **8**(9), 757–760 (2011) [doi:10.1038/nmeth.1652].
5. S. Wolf et al., "Whole-brain functional imaging with two-photon light-sheet microscopy," *Nat Methods* **12**(5), 379–380 (2015) [doi:10.1038/nmeth.3371].
6. F. C. Zanacchi et al., "Two-photon fluorescence excitation within a light sheet based microscopy architecture," in *Multiphoton Microscopy in the Biomedical Sciences XI* **7903**, p. 79032W, International Society for Optics and Photonics (2011) [doi:10.1117/12.879792].
7. J. Palero et al., "A simple scanless two-photon fluorescence microscope using selective plane illumination," *Opt. Express, OE* **18**(8), 8491–8498 (2010) [doi:10.1364/OE.18.008491].
8. Z. Lavagnino et al., "4D (x-y-z-t) imaging of thick biological samples by means of Two-Photon inverted Selective Plane Illumination Microscopy (2PE-iSPIM)," *Sci Rep* **6**(1), 23923 (2016) [doi:10.1038/srep23923].
9. M. Göppert-Mayer, "Über Elementarakte mit zwei Quantensprüngen," *Annalen der Physik* **401**(3), 273–294 (1931) [doi:10.1002/andp.19314010303].

10. K. Wang, N. G. Horton, and C. Xu, “Going Deep: Brain Imaging with Multi-Photon Microscopy,” *Optics & Photonics News, OPN* **24**(11), 32–39 (2013) [doi:10.1364/OPN.24.11.000032].
11. Z. Lavagnino et al., “Two-photon excitation selective plane illumination microscopy (2PE-SPIM) of highly scattering samples: characterization and application,” *Opt. Express, OE* **21**(5), 5998–6008 (2013) [doi:10.1364/OE.21.005998].
12. A. Nag and D. Goswami, “Polarization induced control of single and two-photon fluorescence,” *J. Chem. Phys.* **132**(15), 154508 (2010) [doi:10.1063/1.3386574].
13. I. Micu et al., “Effects of laser polarization on responses of the fluorescent Ca²⁺ indicator X-Rhod-1 in neurons and myelin,” *NPh* **4**(2), 025002 (2017) [doi:10.1117/1.NPh.4.2.025002].
14. K. D. Bonin and T. J. McIlrath, “Two-photon electric-dipole selection rules,” *J. Opt. Soc. Am. B, JOSAB* **1**(1), 52–55 (1984) [doi:10.1364/JOSAB.1.000052].
15. J. R. Lakowicz, *Principles of Fluorescence Spectroscopy*, Springer Science & Business Media (2013).
16. G. Steinbach et al., “Imaging anisotropy using differential polarization laser scanning confocal microscopy,” *Acta Histochemica* **111**(4), 317–326 (2009) [doi:10.1016/j.acthis.2008.11.021].
17. A. Kress et al., “Mapping the Local Organization of Cell Membranes Using Excitation-Polarization-Resolved Confocal Fluorescence Microscopy,” *Biophysical Journal* **105**(1), 127–136 (2013) [doi:10.1016/j.bpj.2013.05.043].
18. A. Gasecka et al., “Quantitative Imaging of Molecular Order in Lipid Membranes Using Two-Photon Fluorescence Polarimetry,” *Biophysical Journal* **97**(10), 2854–2862 (2009) [doi:10.1016/j.bpj.2009.08.052].
19. H. Mojzisoava et al., “Polarization-Sensitive Two-Photon Microscopy Study of the Organization of Liquid-Crystalline DNA,” *Biophysical Journal* **97**(8), 2348–2357 (2009) [doi:10.1016/j.bpj.2009.07.053].
20. N. Vladimirov et al., “Light-sheet functional imaging in fictively behaving zebrafish,” *Nat Methods* **11**(9), 883–884 (2014) [doi:10.1038/nmeth.3040].
21. M. C. Müllenbroich et al., “Bessel Beam Illumination Reduces Random and Systematic Errors in Quantitative Functional Studies Using Light-Sheet Microscopy,” *Front. Cell. Neurosci.* **12** (2018) [doi:10.3389/fncel.2018.00315].
22. “ZFIN Feature: b4,” <<https://zfin.org/ZDB-ALT-980203-365>> (accessed 4 January 2020).
23. F. Maderspacher and C. Nüsslein-Volhard, “Formation of the adult pigment pattern in zebrafish requires leopard and obelix dependent cell interactions,” *Development* **130**(15), 3447–3457 (2003) [doi:10.1242/dev.00519].
24. M. Westerfield, *The zebrafish book: a guide for the laboratory use of zebrafish (Danio rerio)*, 4th ed., Univ. of Oregon Press, Eugene (2000).
25. A. Kuznetsova, P. B. Brockhoff, and R. H. B. Christensen, “lmerTest Package: Tests in Linear Mixed Effects Models,” *J STAT SOFTW* **82**(13) (2017) [doi:10.18637/jss.v082.i13].

Biography

Giuseppe de Vito obtained in 2016 a Ph.D. in molecular biophysics at Scuola Normale Superiore, in collaboration with the Italian Institute of Technology, and a postgraduate diploma in advanced biostatistics at University of Padua. Former junior specialist at University of

California-Irvine, in 2017 he became fixed-term researcher at the Italian National Research Council, before moving in 2019 to the University of Florence. His research focuses on nonlinear optical microscopy of biological samples with different modalities.

Pietro Ricci received his MS degree in experimental physics at the University of Trento in 2018. He then moved to the University of Florence, where he is getting a PhD in atomic and molecular photonics. Since November 2018, he has been working at the European Laboratory for Non-Linear Spectroscopy. His research activity is focused on light-sheet microscopy of zebrafish specimens and multi-beam illumination with acousto-optic deflectors.

Lapo Turrini received his MS degree in biology at the University of Florence in 2015. He then obtained his international PhD in atomic and molecular photonics at the European Laboratory for Non-linear Spectroscopy in 2019. Currently, he is a research fellow at the Department of Physics and Astronomy at the University of Florence. His research activity is focused on whole-brain functional imaging of zebrafish neuronal activity by light-sheet microscopy.

Natascia Tiso received her graduation in biological sciences at the University of Padova in 1994 and her PhD in genetic sciences at the University of Bologna, Italy, in 1998. She has been a visiting scientist at the University of Toronto (Canada), at the MPI of Tuebingen, and at the University of Freiburg (Germany). Currently, she is an associate professor in applied biology and vice-director of the Zebrafish Centre at the University of Padova.

Ludovico Silvestri received his MS degree in physics in 2008 at the University of Pisa and his PhD in atomic and molecular spectroscopy at the University of Florence in 2012. He worked as postdoc at LENS until 2014, then as Researcher at the National Institute of Optics until 2019. Currently, he is an assistant professor at the Physics and Astronomy Department of the University of Florence. His research activity is focused on light-sheet microscopy of cleared specimens.

Francesco S. Pavone is developing new microscopy techniques for high-resolution and high-sensitivity imaging and for laser manipulation purposes. These techniques have been applied to single-molecule biophysics, single-cell imaging, and optical manipulation. Tissue imaging is another active research area, where nonlinear optical techniques have been applied for skin and neural tissue imaging, also *in vivo*.

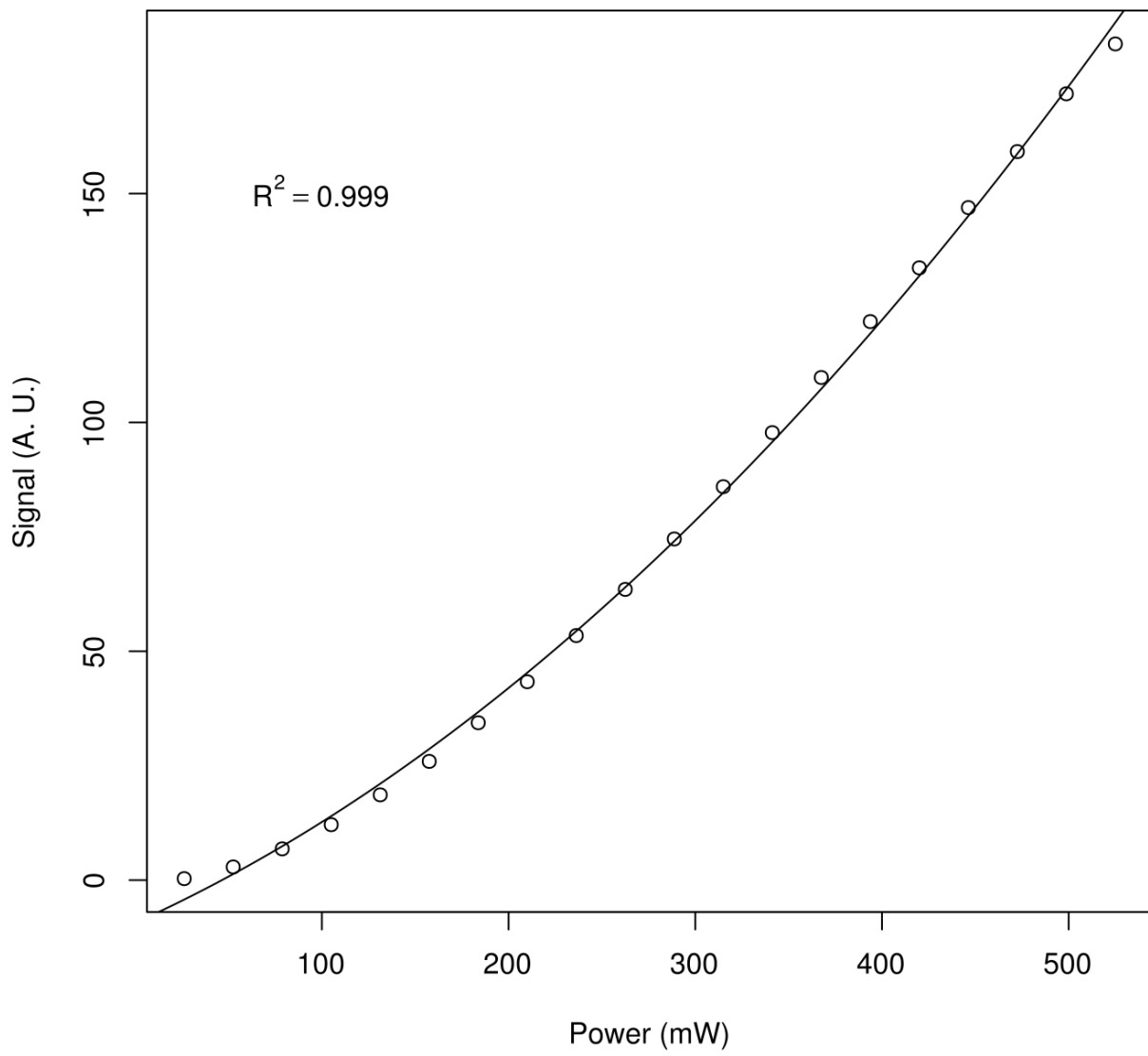


Fig. S1 Scatter plot of the fluorescent signal generated by a fixed Tg(actin:EGFP) larva as a function of the excitation power. Parabolic fit of the data is indicated by the continuous line and its coefficient of determination is reported on the graph.